

1 Article

2 Automatic Crack Detection of Road Pavement Based 3 on Aerial UAV Imagery

4

5 **Farzaneh Dadrasjavan** ^{1,*}, **Nima Zarrinpanjeh** ² and **Azam Ameri** ¹

6 ¹ School of Surveying and Geospatial Engineering, University College of Engineering, University of Tehran,
7 Iran; {fdadrasjavan,a.ameri}@ut.ac.ir

8 ² Department of Geomatics Engineering, Qazvin Branch, Islamic Azad University, Qazvin, Iran;
9 nzarrin@qiau.ac.ir

10 * Correspondence: fdadrasjavan@ut.ac.ir;

11 **Abstract:** Road surface monitoring more specifically crack detection on the surface of the road
12 pavement is a complicated task which is found vital due to critical nature of roads as elements of
13 transportation infrastructure. Cracks on the road pavement is detectable using remotely sensed
14 imagery or car mounted platforms. UAV's are also considered as useful tools for acquiring reliable
15 information about the pavement of the road. In This paper, an automatic method for crack detection
16 on the road pavement is proposed using acquired videos from UAV platform. Selecting key frames
17 and generating Ortho-image, violating non road regions in the scene are removed. Then through an
18 edge based approach hypothesis crack elements are extracted. Afterwards, through SVM based
19 classification true cracks are detected. Developing the proposed method, the generated results show
20 75% accuracy in crack detection while less than 10% of cracks are omitted.

21

22 **Keywords:** Crack Detection; UAV Imagery; SVM Classification; Aerial Photogrammetry

23

24 1. Introduction

25 Monitoring of Infrastructures and lifelines is believed to be a never ending story. As a matter of
26 fact, the prominence of those facilities totally rely on perpetual and constant observance and
27 evaluation of functionality of their elements. An undetected failure in water supplement in a
28 populated region or any damage to main highways directly and immediately affects the life of
29 residence. Therefore, a well- defined economic and efficient monitoring method for each and every
30 important infrastructure and lifeline is believed to be vital.

31 Roads network are of the most prominent infrastructure that are systematically classified under
32 the category of transportation lifelines. As Roads are the main transportation mean around the world,
33 carrying goods and services is mostly based on developed and functional system of roads network.
34 Roads are required to be functional almost every time. This eventually imposes tight minoring of the
35 facility. On the other hand, due to the roads' distributed and elongated nature, the process of
36 monitoring seems to be time consuming and expensive procedures. According to American
37 Association of State Highway and Transportation Officials, maintenance of road cost more than 67 B
38 US dollars annually (koch et al., 2015).

39 Roads are also vulnerable due to natural causes and disasters. Regardless of the more complex
40 structures such as bridges and tunnels, the pavement of roads are also affected by natural and man
41 caused events. Cracks are of the common damages to road pavement occurring mostly due to the
42 constant change in temperature, weight of vehicles, erosion and chemical corruptions (Behnia et al.,
43 2018). Consequently, crack monitoring seems to be promising to analyze and evaluate the current
44 condition of roads. Quality, shape, type, depth and length of cracks are some of the most measures

45 in crack analysis and monitoring (Mohan and Poobal, 2018). Therefore, acquiring reliable information
46 about cracks on the surface of the roads seems to be vital for efficient maintenance of the road
47 network.

48 The simplest method to inspect road surface is the visual inspection at the location which is
49 considered to be inefficient and expensive. On the other hand, remote sensing techniques are believed
50 to be one of the most suitable and reliable solutions for monitoring and maintenance of such facilities
51 which are found interesting in nineties. With the advent of technology and the appearance of new
52 imaging sensors, the concept of image based monitoring of roads has peeled and evolved. One of the
53 most brilliant tools are Unmanned Airborne Vehicles also referred to as UAVs. Regardless of the
54 diverse applications of UAVs, they are practically bolded in the process of acquiring high resolution
55 imageries which facilitates more detailed inspection and monitoring through a safe and economic
56 procedure (Aldea et al., 2015; Grandsaert, 2015; Sankarasrinivasan et al., 2015).

57 In this paper reviewing the most recent and the most important researches about crack detection
58 from different sensors, a method to detect and extract asphalt cracks of roads using UAV based
59 imagery is defined.

60

61 **2. Crack Detection from Airborne Imagery**

62 Automatic crack detection from imagery is categorized with respect to the data acquisition
63 perspective and processing method (Coenen and Golroo, 2017). Considering data acquisition
64 platform, three main imaging methods of terrestrial, Aerial and satellite images are used for remote
65 sensing based crack detection. In terrestrial case, image acquisition systems are usually mounted on
66 a moving vehicle such as cars and trains usually categorized under mobile mapping terms (Quintana
67 et al., 2015). Airborne and satellite imaging systems are other information providing sources for crack
68 detection (Schnebele et al., 2015). Due to the limitations of satellite imagery to provide sufficient
69 spatial resolution, airborne systems and recently UAV based imaging systems are widely used for
70 crack detection.

71 Crack detection techniques from images are mostly performed in four stages of preprocessing,
72 segmentation, classification and enhancement. At the preprocessing level, basic enhancement
73 techniques such as noise reduction, smoothing, sharpening and edge detection along with some more
74 complex processing including removal of misleading and violating objects such as cars, vegetation,
75 shades, signs and marks are performed. In the segmentation step, candidate crack primitives are
76 extracted mostly based on the similarity of cracks to edge elements. In the next step classification is
77 performed to define crack region and finally the results are enhanced mostly through morphological
78 filtering (Cubero-Fernandez, 2017; Gavilan et al., 2011;).

79 Yokoyama et al., 2017 presented an automatic crack detection technique training artificial
80 neural networks. The results showed in case of classification in two classes of crack and non-crack,
81 the algorithm success rate in 79.9 %. In case of three classes of cracks, non – cracks and white lines,
82 this method is 73.3 percent successful. It is also concluded that the method is successful in case of
83 monitoring the stainless paved surfaces but inspecting concrete surfaces the successfulness of the
84 method drops drastically.

85 Kim et al., 2017 proposed a crack detection method based on integrating different image analysis
86 methods using both imagery and ultra-sonic sensors to measure distance. They focused on discrete
87 crack and the main objective of paper was to measure length and width of cracks. The proposed
88 system showed the successful detection of cracks thicker than 0.1 mm with the maximum length
89 estimation error of 7.3%.

90 Cubero-Fernandez et al., 2017 presents a crack detection technique using edge detection and
91 morphological operations. In this research after preprocessing of spatial data through noise reduction
92 and smoothing, canny edge detection is applied. The results are enhanced through morphological
93 closing for gap removal. Finally, through a decision tree the success rate of 88 % is achieved.

94 Ersoz et al., 2017 proposed a method extracting crack in two steps of segmentation and
95 classification using images of a low traffic road segment. Thresholding the results, the remaining

96 noise is removed via closing operator. SVM classifier issued to make distinguishes between cracks
97 and non-cracks items considering geometric features. The accuracy of 97% was achieved where the
98 flight was too low inspecting concrete surfaces.

99 Yin et al., 2015 proposed a crack detection technique by creating image pyramid of the acquired
100 UAV images and performing canny edge detection in multiple scales. Final edges representing cracks
101 are detected by aggregating the results of crack detection in different scales.

102 In Aldea and Le Hégarat-Mascle, 2015 crack detection is studied based on two algorithms of
103 minimum path cost analysis and image percolation. Moreover, an improved strategy based on a-
104 contrario modeling which able to withstand the significant motion blur is proposed. Experimenting
105 the proposed method on real image databases, the results showed that the proposed method is
106 successful compared to other similar solution which only work on perfect images and not of
107 significantly degraded images.

108 Chamben et al., 2010 considers a simulated imagery for crack detection. In this approach Markov
109 model and adaptive filtering are used for segmentation and crack detection. In this paper it was
110 attempted to explore the best configuration of parameters considering Markov field direction and
111 window size.

112 Oliveira et al., 2009 proposed a complete workflow for detection and categorization of road
113 surface cracks using imageries from road monitoring vehicles in a fast solution. Morphological
114 operation is used to reduce noise and through dynamic thresholding cracks are generated. Evaluating
115 the results, success rate of 95 percent is achieved.

116 Sankarasrinivasan et al., 2015 proposed an innovative protocol for full field mapping of a large
117 civil structures involving effective use of Unmanned Aerial Vehicles to enable real time structural
118 health monitoring. The proposed framework integrates UAVs, image processing and acquisition
119 procedures for crack detection and assessment of surface degradation. A novel approach is proposed
120 combining hat transform and HSV thresholding technique for crack detection. In addition, grey scale
121 thresholding is employed for the measurement of surface degradations .The demonstrative model is
122 proven to be reliable and feasible for full field mapping and health monitoring for civil
123 infrastructures.

124 In summary, it is obvious that remote sensing based methods of crack monitoring usually result
125 in satisfying results in case of time and cost and among them UAV based imageries prompt to be
126 more interesting in recent years. In image processing based methods, pre-processing step is crucial
127 for achieving higher accuracy in final results, otherwise, the results are promising, but they are
128 affected by spots or shadows.

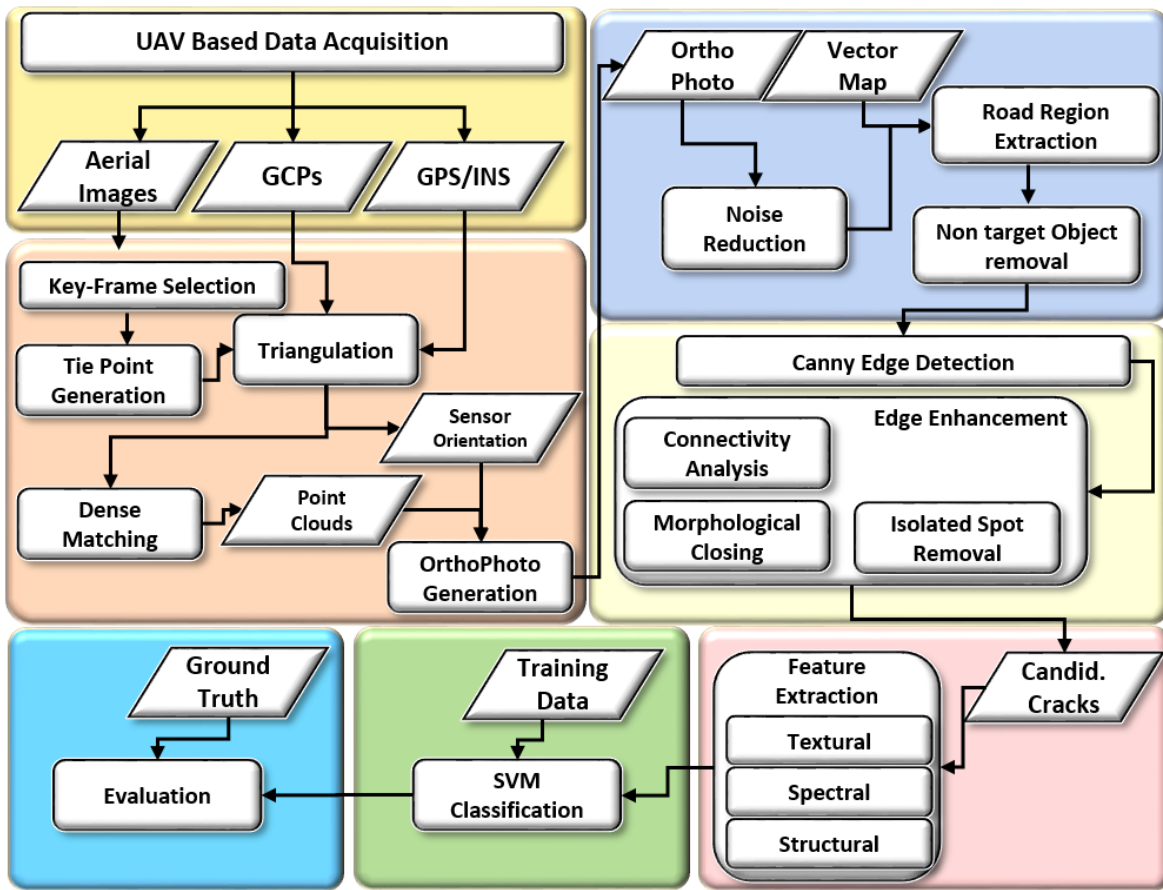
129 Up to now, a few image based crack detection methods have been studied and proposed
130 specially for UAV based imagery. Most of these studies are focused on cracks in concrete surfaces
131 or simple data sets. In this study we proposed an automatic method for asphalt crack detection in
132 roads which are highly involved with violating objects, noises, spots and so on.

133

134 3. Proposed Crack Detection Method

135 Considering the capabilities of information UAV imaging systems provide and on the basis of
136 the researches developed for crack detection in various applications, the proposed method for
137 automatic crack detection is presented. As illustrated in figure 1, the proposed method is comprised
138 of six levels of action. At the first level, aerial imageries along with simultaneous record of onboard
139 GPS/INS measurements of Exterior Orientation parameters and also GCPs are acquired. In the next
140 level, through photogrammetric computation, digital Ortho-Image of the region is generated. Next,
141 in preprocessing section noise reduction, image enhancement and removal of non-crack objects such
142 as vegetation, cars and shades are performed. Through candidate crack detection, a set of hypothesis
143 cracks primitives which enjoy structural similarity to typical cracks are generated using edge
144 detection techniques. In the next level, to verify the true cracks, best features to utilize in classification
145 process are computed and assessed. Then, SVM classification is used to determine final cracks and a

146 modification process is proposed. Finally, in the evaluation step, the results are compared with
 147 respect to ground truth collected by expert.
 148



149
 150 **Figure 1.** the flowchart of the proposed automatic crack detection method from UAV images

151 3.1. UAV Based Imaging and Data acquisition

152 As roads are elongated regions, the use of light multirotor and light sensors with high mobility
 153 and lower flight altitude and speed are considered. To fortify the process of sensor orientation,
 154 onboard GPS/INS information are used. To improve the spatial accuracy of the final map of cracks,
 155 GCPs are acquired through ground surveying.

156 The most important fact about choosing most suitable UAV and sensor is the imaging speed
 157 which is related to the sensor speed and UAV altitude and speed. Too low speed increases the project
 158 cost and too high speed will result in blurriness of images. On the other hand, the resolution of final
 159 achieved images should be considered in advance at the flight planning step. The optimum resolution
 160 depends on the width of cracks, if it's less than 3 pixels, the line extraction methods can be applied.
 161 Therefore, it should be defined in a way to provide optimum size of crack in images and also prevent
 162 data redundancy. The flight time is also important in order to prevent large shades which might
 163 result in occluded area.

164 3.2. Key-frame Extraction

165 As the sensor used is a video acquisition sensor, after data acquisition, key frames have to be
 166 extracted. Key frames can be selected based on radiometric and geometric aspects. In radiometric key
 167 frame selection, the quality of the frames is checked and the blur low content frames are removed;
 168 but in geometric key frame selection, the frames are checked for geometrical stability vital for
 169 photogrammetric processing.

170 In this study, for radiometric frame selection, the BluM metric is applied. The output of this
 171 algorithm is a score between 0 to 1. Results close to 0 represent the best and results close to 1 represent

172 the worst sharpness of images, respectively. Using a predefined threshold, acceptable and non-
173 acceptable frames are selected (Crete et al., 2007; Arofteh et. al., 2017).

174 Geometric Robust Information Criterion (GRIC) factor which is presented by Torr et al. (1996) is
175 applied for geometrical evaluation of frames. GRIC evaluates which of the Fundamental epipolar
176 geometry model (F) or homography model (H) is best suited to explain the geometrical relation of
177 two sequences (Arofteh et. Al., 2017). GRIC is defined as:

$$GRIC = \sum_i \rho(e_i^2) + \lambda_1 dn + \lambda_2 k \quad (1)$$

178 and

$$\rho(e_i^2) = \begin{cases} \frac{e^2}{\sigma^2} & \frac{e^2}{\sigma^2} < \lambda_3(r - d) \\ \lambda_3(r - d) & \frac{e^2}{\sigma^2} \geq \lambda_3(r - d) \end{cases} \quad (2)$$

179 Where d = Dimension of the selected motion model (H has the dimension two and F has
180 dimension three); r = Dimension of the data (i.e. four for two views; k = Number of the estimated
181 model parameters (seven for F and eight for H); n = Number of tracked features; σ = Standard
182 deviation of the error on each coordinate; e_i = Distance between a feature point transferred through
183 H and the corresponding point in the target image or the Euclidian distance between the epipolar line
184 of a feature point and its corresponding point in the target image.

185 The GRIC has used for key frame extraction with tuning parameters of λ_1 . λ_2 and λ_3 with:

$$\lambda_1 = \ln(r). \quad \lambda_2 = \ln(rn). \quad \lambda_3 = 2 \quad (3)$$

186 In practice, to avoid selecting too many key-frames, it is proposed to pick a key-frame at the last
187 frame for which:

$$ni \geq 0.9ne \quad (4)$$

188 where ni = Number of valid tracked features; ne = Number of valid tracks when the Epipolar
189 geometry model overtakes the Homography model.

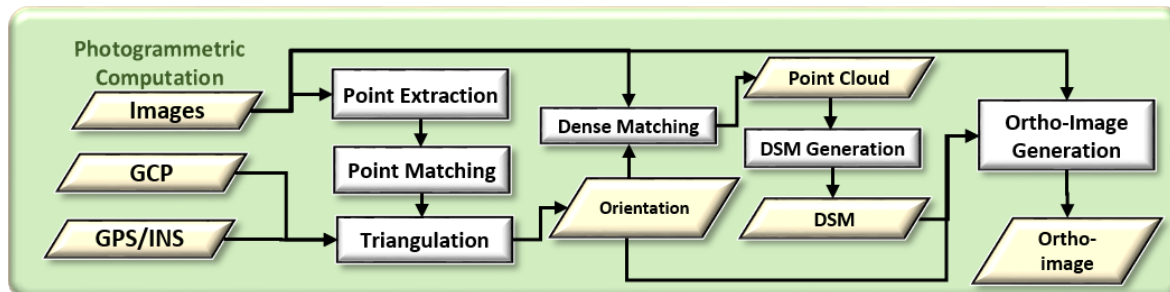
190 After initializing the first frame of the sequence as key-frame and proceeding frame by frame,
191 the next key-frame is selected if the GRIC value of the motion model F is less than the GRIC value
192 of H .

193

194 3.3. Photogrammetric Computation

195 In the photogrammetric computation, the acquired imagery and extracted frames are elaborated
196 to digital Ortho-image. The process as it is so called Structure From Motion (SFM) starts with the
197 extraction of tie points in imagery using image matching usually being performed automatically
198 through point extraction and matching algorithms. Then, block bundle self-calibration is performed,
199 firstly to estimate interior and exterior orientation parameters of images and secondly to estimate 3D
200 ground coordinates of tie points. Then, through dense matching algorithm, Digital Elevation Model
201 of the region is generated. Using a backward projection technique, the Digital Ortho-photo is
202 generated. The flowchart of Photogrammetric Computation step is depicted in figure 2.

203



204

205 **Figure 2.** Ortho image generation through Structure from motion procedure.

206 *3.4. Preprocessing*

207 The preprocessing section considers two phases of low and high level preprocessing procedures.
208 In the low level process, noise reduction or any further image enhancement and filtering is applied.
209 High level preprocessing includes the removal of non-road regions or regions where the existence of
210 any crack is impossible or improbable or simply not required. In other words, the road region in the
211 digital Ortho-image could be inspected for road regions which is mostly applicable by overlaying
212 digital maps of the road and masking target road regions. On the other hand, there are some non-
213 road objects on the surface of the road which may violate the process of crack detection. In this case
214 violating non target objects such as cars, shades and signs are removed.
215

216 *3.4.1. Image Enhancement and noise removal*

217 In order to reduce the noisy content of image and to enhance the image in a way that the cracks
218 become more distinctive than the background, this study proposed a combination of smoothing filter
219 and top hat and bottom hat operation based on relation (5).
220

$$F = ((SH + \text{tophat}(SH)) - \text{bothat}(SH)) \quad (5)$$

221 where F is the enhanced image, SH is the input image which is smoothed based on a Gaussian
222 filter.

223 *3.4.2. Removing Marginal Non- Road Regions*

224 In this step, roads regions are extracted from the scene so the process of crack detection is only
225 conducted on the road region to decrease the amount of unnecessary computation and false positive
226 detections. Therefore, road network is projected on the Ortho-image and according to the width of
227 the road segment, the corresponding road regions are extracted. It should be noted that the quality
228 of generated Ortho-image and the accuracy of road network has direct impact on the extracted road
229 region. Therefore, an accurately generated Ortho-image and updated accurate vector road network
230 is necessary.
231

232 *3.4.3. Removing Non target disturbing objects*

233 Road surface presented in the digital Ortho-image is always violated by occlusions imposed by
234 the scene configuration of objects. The existence of vegetation, cars, signs and lines, shades and
235 occlusion from neighboring elevated objects such as buildings, may disturb the process of crack
236 detection through increasing high frequencies to the digital imagery and increasing the number of
237 detected edges and as a results increasing the percentage of False Negative detections.
238

Threshold applying is the main tool to remove most of the violating objects. For vegetation
239 removal NDVI in case the Ortho-image enjoys Infra-Red channel or Greenness value where only RGB
240 channels are available, are often used (Samadzadegan and Zarrinpanjeh, 2008). For shade removal
241 the same procedure considering illumination in IHS space along with Hue value is used. For car
242 detection, morphological geodesic filtering is believed to be promising [Zarrinpanjeh and
243 Dadrassjavan, 2017]. In this case the size of extracted cars is inspected with respect to conventional
244 car sizes.

245 *3.5. Crack primitive detection*

246 The process of crack primitive extraction in this research is mainly based on edge detection
247 techniques. As cracks appearing on the surface of the road pavement demonstrate sudden changes
248 in grey value, it is reflected through high frequencies in the imagery. It should be noted that as high

249 frequencies appear in the form of various objects such as dots and ramps, the most important
 250 elements in choosing proper detector is extremely vital. According to the linear characteristic of
 251 cracks Canny edge detection is used as a solution (Gonzalez and Woods, 2002).

252 To enhance detected cracks, Connected Component Analysis and Top-Hat morphological
 253 filtering are performed. This makes the extracted candidate crack primitives to be enhanced and
 254 considered as an image objects rather than pixels. Because the results of edge detection are supposed
 255 to be accompanied by similar linear objects such as lines and repaired pavements, crack enhancement
 256 helps removing the scattered non-crack edges. Nevertheless, the detected edges also include false
 257 cracks that should finally be verified. Smoothing and morphological filters might help removing
 258 these artifacts but they might remove sections of cracks as well. As a result, a sliding window filtering
 259 method is proposed in this study. Based on the proposed strategy, a window with size smaller than
 260 the smallest crack size of the dataset is sliding through the whole image and any objects fully
 261 bounded by this window is removed.
 262

263 *3. 6. Crack and non-crack classification*

264 After extraction of crack primitives those are considered as the candidate cracks are introduced
 265 to classification process to define the true cracks and to remove false positives. The classification
 266 process is composed of two main stages as feature extraction and SVM classification of extracted
 267 features.
 268

269 *3.6.1. Feature extraction*

270 To consider SVM classifier to distinguish between crack and non-crack hypothesis primitives,
 271 a list of features is considered and computed. In this research, a set of spectral, textural and structural
 272 features are studied and used. Table (1) defines the feature to be computed for inspection of
 273 extracted candidate cracks.
 274

275 **Table 1.** Feature for Crack detection from satellite imagery.

Feature		Description
Spectral	R,G,B	Red, Green, Blue Channels of the Digital Ortho-image
	Mean	Mean value of spectral bands
Textural	Contrast	Contrast of the neighborhood Box of the evaluated pixel
	Correlation	Contrast of the neighborhood Box of the evaluated pixel
	Energy	Computes the energy of the neighborhood Box [haralick]
	Homogeneity	Computes the Homogeneity of the neighborhood Box [haralick]
Structural	Extent	The area of the Bounding Box of the Crack
	Eccentricity	The eccentricity value of the Bounding ellipse
	Minor axis Length	The Minor axis length of the bounding ellipse
	Major axis Length	The Major axis length of the bounding ellipse
	Orientation	The angle of the major Axis with respect to horizontal axis

276
 277 Features used in this research are mostly chosen by inspecting the specification and
 278 characteristics of cracks. Therefore, more structural features are chosen rather than spectral where
 279 the spectral difference of cracks compared to non-crack paved regions is not so prominent.
 280

281 *3. 6.2. SVM Classification*

282 Training regions are extracted and SVM classifier is used for classification of candidate cracks.
 283 Training the SVM classifier, all candidate cracks are introduced to the trained SVM and the extracted

284 candidate cracks are evaluated. As SVM is defined to classify patterns in two classes, it is found
 285 suitable to detect cracks from non-cracks objects in this application (Cortes and Vapnik, 1995).
 286

287 *3.7. Evaluation*

288 To evaluate the successfulness of the results, two levels of evaluation is proposed. In the first
 289 one, the capability of SVM classifier in being trained by the training data is evaluated based on the
 290 test data set. The test data set is a random selection of pixels as test and training data. Moreover, for
 291 accuracy assessment of the result of the proposed automatics crack detection method, they are
 292 compared to the cracks detected manually by the expert as independent ground truth.
 293

294 **4. Results**

295 To experiment the capabilities of the proposed method in successful detection and mapping of
 296 the cracks in the road pavement, the proposed method is implemented and tested for UAV based
 297 aerial imagery and the generated results are evaluated and discussed.
 298

299 *4.1. UAV based Image Acquisition*

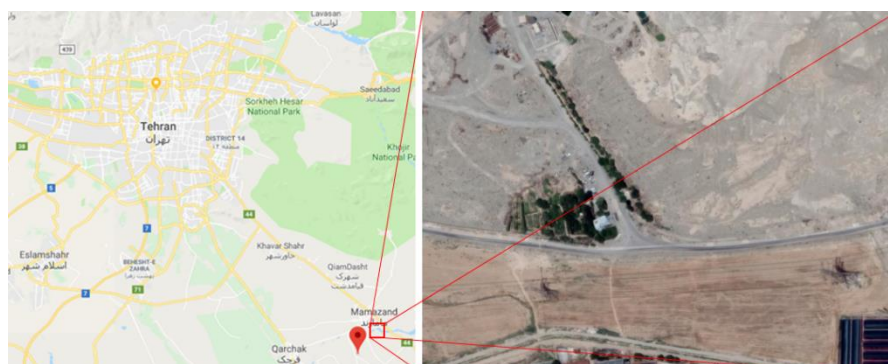
300 For image acquisition, a multirotor UAV equipped with a GoPro4 camera and GPS/IMU systems
 301 is used. Table (2) defines the specifications of the platform. Images are acquired from a road in south
 302 east of Tehran, Iran. The overall view of selected road and the summary of flight plan parameters are
 303 provided in figure (3).
 304

Table2: The aerial platform specification

Flight Endurance	40 min
Max Flight Height	2000m
Dimension	1.2 m
Optimum Speed	20 km/h



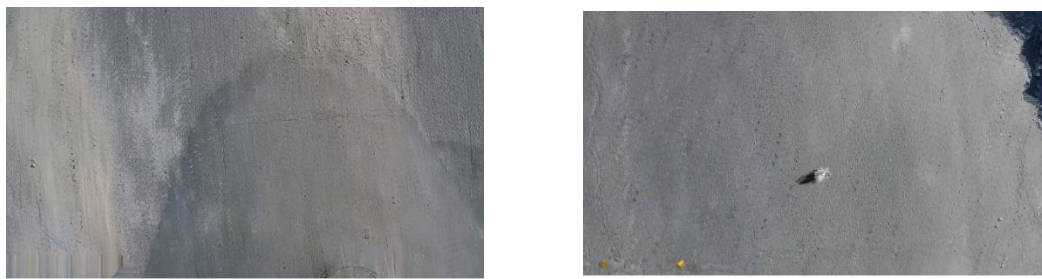
305



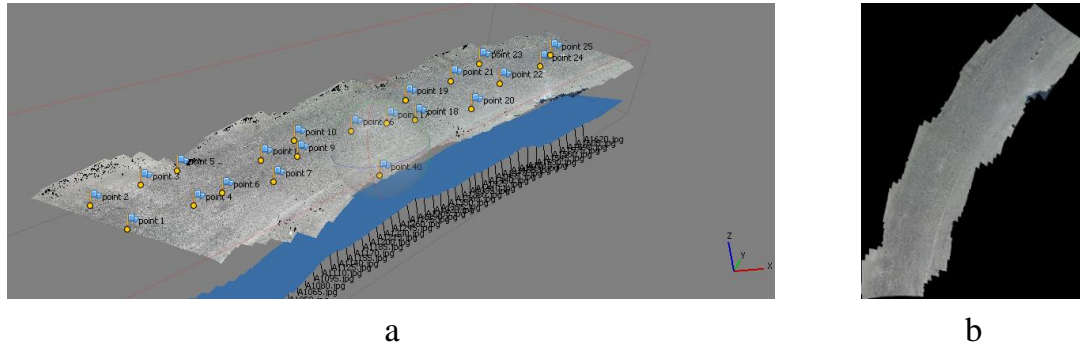
Flight Time	10 min
Flight Height	60 m
CSD	3.6 cm
Flight Speed	20 km/h

Figure 3. Data set and flight plan parameters306 4-2- *Key-frame selection*

307 To execute photogrammetric process key frames are selected from video string and images
 308 suffering from lower quality in terms of illuminance, focus and motion blur are removed. Moreover,
 309 to prevent data redundancy, key frames are selected based on geometrical stability for bundle block
 310 adjustment based on GRIC algorithm. Figure 4, shows some samples of rejected frames.

**Figure 4.** Samples of rejected frames according to BluM procedure.311 4-3- *Photogrammetric Computation*

312 As a result of key-frame extraction step, images with minimum 70 percent overlap are selected
 313 those are higher in quality and enjoy stable epipolar geometry. Conducting the photogrammetric
 314 procedure, the ortho-image of the region is generated. Figure 5, illustrates the camera position and
 315 generated ortho-image. The block bundle adjustment is conducted with the accuracy of 0.01 meters.

**Figure 5.** a) Photogrammetric process of selected images b) resulted digital Ortho-image.316 4-4- *Preprocessing*317 **Image enhancement and noise removal**

318 In the first step of image preprocessing, image enhancement is applied to reduce noise content
 319 of images and also to enhance the image for crack detection based on Canny operation. For the
 320 purpose, image is firstly smoothed based on Mean filter and then the combination of Top Hat and
 321 Bottom Hat operation is applied as discussed previously. The parameters for these operators are set
 322 as SE = 3, Sigma = 0.2 and Hsize = 5.
 323

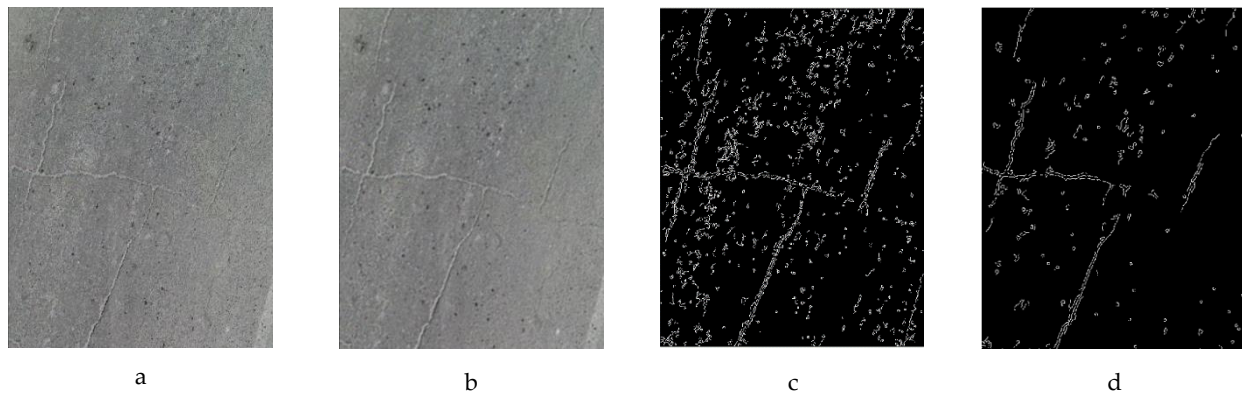


Figure 6. a) Original Image; b) Results of Smoothing step; c) Results of Canny edge detection; d) results of canny Algorithm after Top Hat operation

324 **Non-target removal**

325 In this step, non-target regions violating the process of crack detection are omitted. At first, the
 326 road segment of image is extracted and the back ground is removed. This process is based on the pre-
 327 information about the road map and the width of road based on scale of image. Figure (7) presents
 328 the result of road extraction process. The accuracy of this step is evaluated based on the map
 329 generated by digitizing the ortho-image by expert which is determined as 97 percent. The main
 330 reason of the lower accuracy is the vegetation covering the marginal part of the road which is also
 331 removed based on threshold applying on the Red band of images. Doing so, the final quality
 332 increased to 98.8 percent. The road white lines can also be removed easily based on applying
 333 threshold.

334

335



Figure 7. a) Original image; b) road extraction and white line filtering; c)vegetation filtering

336 The point that might challenge the automatic extraction of cracks is the margin of road after
 337 extraction of road from the back ground. This margin should be removed from the image before crack
 338 detection process. In figure (8) results of this step is presented. The operation of Canny line extractor
 339 before and after this step is also presented to prove the necessity of this process.

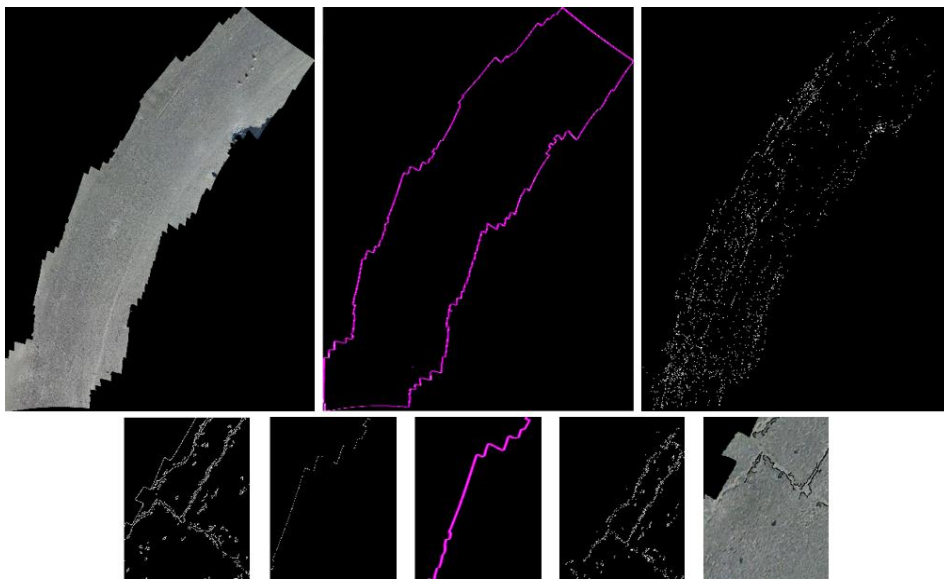


Figure 8. road margin removal

340 The large shadows on the road are also non objects elements that might violate the crack
 341 detection process. For the purpose, shallows are removed based on applying threshold value and
 342 remaining isolated small objects are also removed based on morphological filters. Results are
 343 presented in figure (9). The successfulness of this process is also evaluated based on expert generated
 344 data.

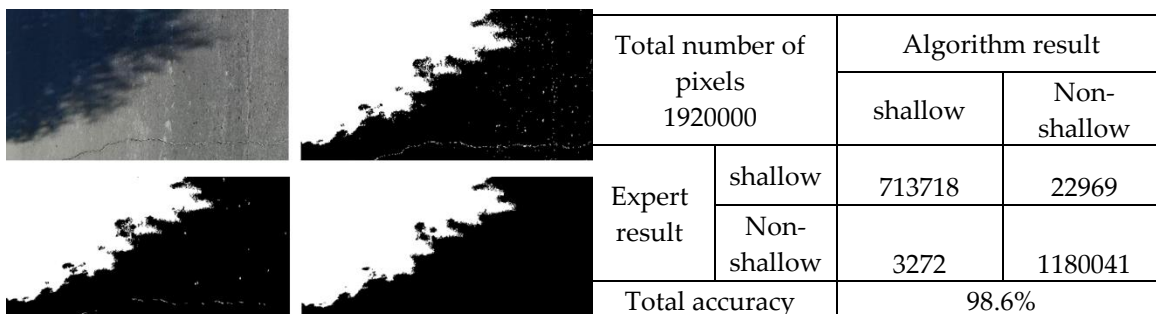


Figure 9. shallow removal and the accuracy assessment

345 Cars and large non targets elements are also removed by applying geodesic filter following by a
 346 closing morphological filter with the accuracy of 97.7%. Results are presented in figure (10).
 347

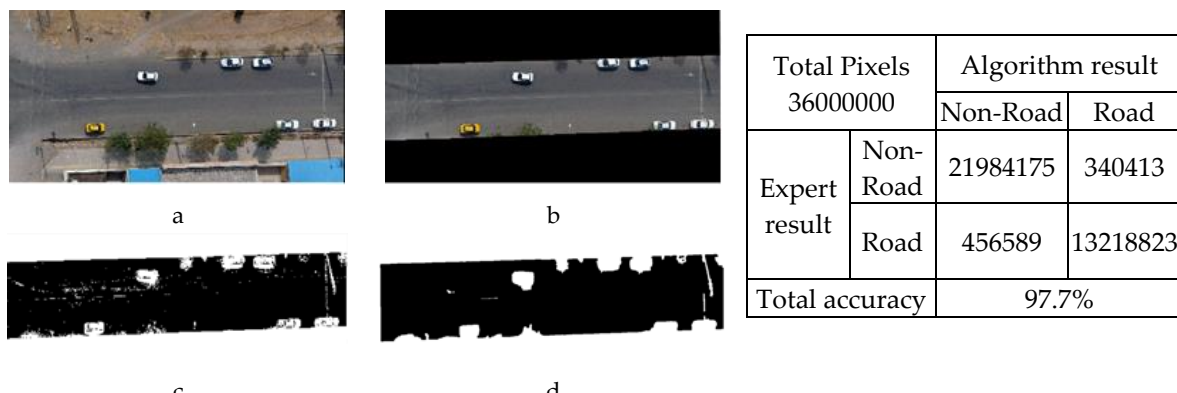


Figure 10. Cars and big objects removal and the accuracy assessment

348 4-5- Crack primitive extraction

349 After extraction of road and removing the non-target elements, Canny edge detection technique
 350 is executed and edges are extracted. Through proposed Top-Hat algorithm and the recursive window
 351 sliding process, results are enhanced and as it is depicted in figure 11, the results are more similar to
 352 cracks through visual inspection, compared to the unfiltered ones, as most of noises which may cause
 353 false crack detection are removed. Afterwards, using morphological operation, extracted edges are
 354 combined as distinctive objects and are introduced to next processing step as candidate cracks.
 355

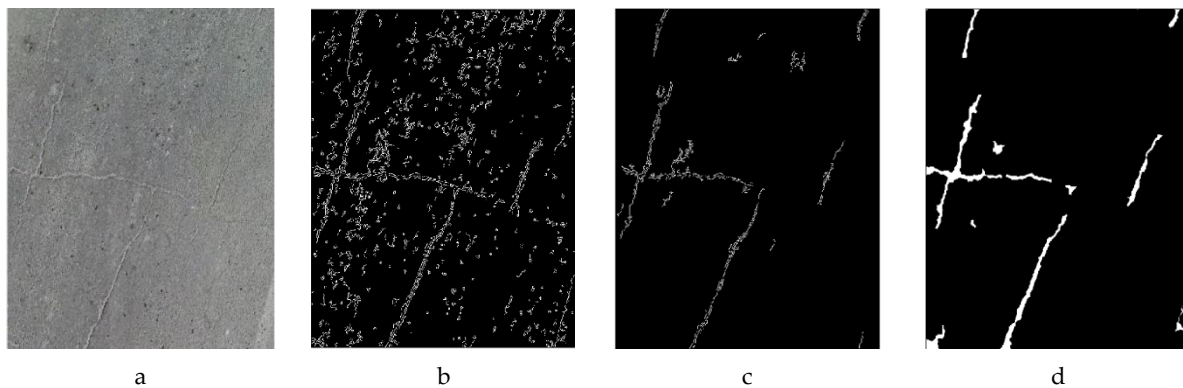


Figure 11. a)Original Image; b) Results of Canny edge detection; c) results of canny Algorithm after filtering process; d) final crack candidate elements

356 4-6-Crack and non-crack classification

357 By extraction of crack candidates, the test and training data are prepared. The training data are
 358 gathered in two different solution of object based and pixel based as it is depicted in figure (12).

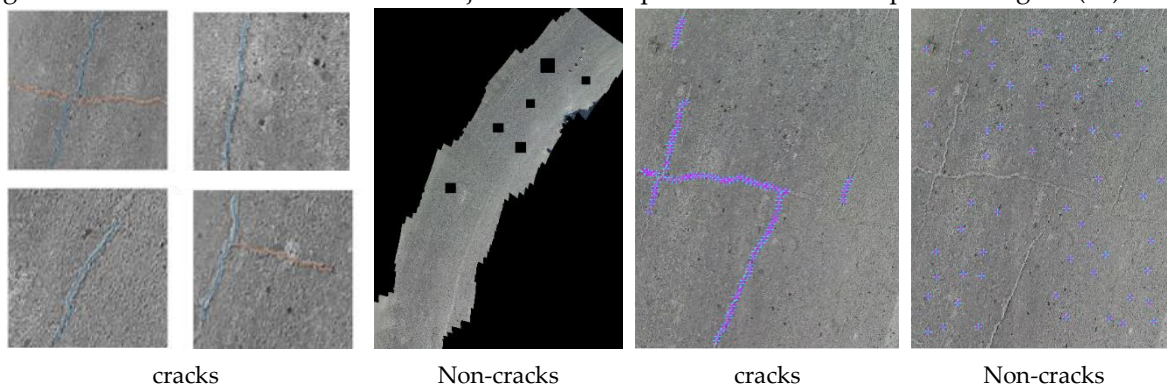
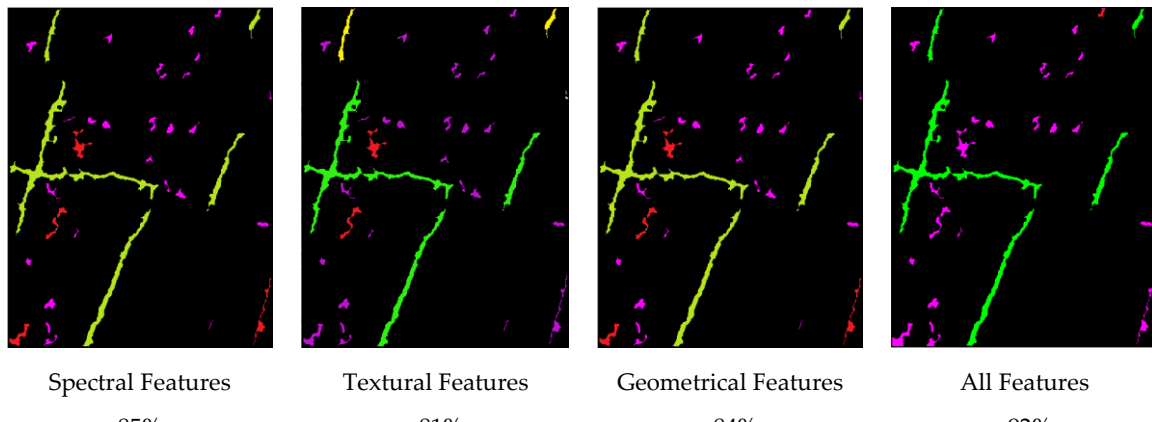


Figure 12. training data generation, left) object based; right) pixel based strategy

359 After definition of training and test data sets, candidate cracks are introduced to the SVM
 360 classifier. For the classification process, 4 different scenarios of feature selection are implemented and
 361 evaluated as Spectral/Textural/Structural and the combination of all features. Achieved results are
 362 presented in figure (13).



Green: cracks; Violet: Non-cracks; Red: Non-cracks labeled as cracks; Yellow: cracks labeled as non-crack

Figure 13. SMV classifier results

363 In order to improve the results of classification, object level post-processing of results is
 364 considered. In this strategy, after classification of the pixels of candidate cracks, the pixel content of
 365 each object (candidate crack) is evaluated. By considering the majority and minority condition, the
 366 object as a whole is labeled instead of the pixels. Figure (14) depicted the labeling rule in this content.
 367 Based on this strategy, the accuracy of test data improved from 87% to 92%.
 368
 369

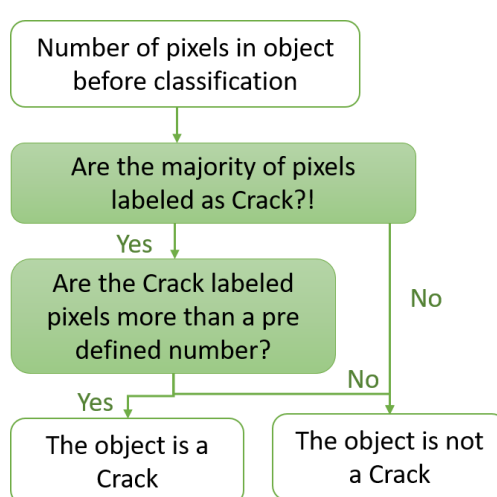


Figure 14. Object based assessment of cracks

370 4-7-Evaluation of results

371 Final results of the proposed crack detection strategy for the whole study area are presented in
 372 figure (15). The validity assessment of the results is performed based on the ground truth extracted
 373 by the digitizing process of an expert for the whole study area which is presented in table (3).
 374

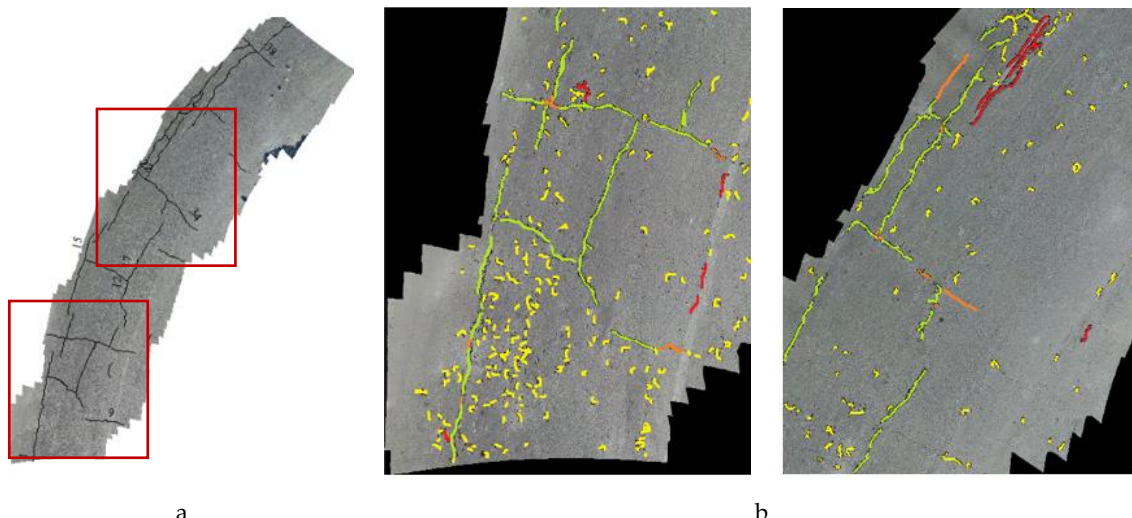


Figure 15. Final Crack detection result, a) the ground truth; b) samples of crack detection results, Green: cracks; Yellow: Non-cracks; Red: Non-cracks Labeled as Cracks; Orange: Cracks labeled as Non-crack

Table 3. The validity assessment of the results.

Total Pixels 237735		Algorithm Results	
		Crack	Non-Crack
Expert Results	Crack	105012	22892
	Non- Crack	34955	73076
Total accuracy		74.9%	

375 5. Discussion and Conclusion

376 Few methods have been proposed to detect cracks from drone images, while there is no certain
 377 method which can detect all cracks, automatically. Previous study mostly focused on images taken
 378 from concrete structures or by road health monitoring vehicles. These images are high in quality and
 379 cracks are usually more prominent than aerial images acquired from roads with asphalt surface.

380 In automatic crack detection, pre-processing is an important step which plays a critical role in
 381 removing violating elements and also decreasing the processing time and cost. Road extraction,
 382 image smoothing, noise removal and non-target elements removal are the pre-processing steps
 383 discussed in this study.

384 Moreover, the candidate crack detection is the next step works as pre-crack detection and
 385 enhancement. For the enhancement of detected pre-cracks, a recursive strategy based on a sliding
 386 window checking extracted objects is proposed which improve the results by removing small non
 387 crack objects prominently.

388 For final classification of candidate cracks in two classes of cracks and non-cracks, SVM classifier
 389 with three spectral, textural and geometrical feature classes is applied. Results on test data presented
 390 that using textural features leads to the lowest accuracy as 81% which is predictable because the
 391 textural behavior of cracks are not very different from other parts of image specially in asphalt based
 392 roads. Moreover, applying spectral and structural features separately resulted in the accuracy about
 393 85% which is the result of different behavior of cracks in color and shape with respect to non-cracks
 394 parts. Finally, applying all the spectral, textural and structural features improve the accuracy on the
 395 test data up to 92%.

396 Moreover, the object level process, which consider the cracks based on Connected Component
 397 Analysis as an object, helps to improve the accuracy from 87% to 92%.

398 Finally, the reliability analysis of the proposed strategy was applied based on the ground truth
399 data generated by expert. Results showed the final accuracy of 74.9%. Although this value seems not
400 interesting enough, but considering the complexity of aerial imagery and the non-uniformity texture
401 and variety in shape, size and look of cracks in asphalt roads surface, it could be acceptable for an
402 automatic process. Moreover, results presented that less than 10 percent of cracks are lost, which
403 means that the algorithm missed only a few number of cracks. This failure rate in comparison with
404 the time and cost of the expert based and mobile vehicle based monitoring methods, presents the
405 superiority of the proposed UAV based automatic monitoring of cracks.
406

407 References

408 Aldea, E., & Le Hégarat-Mascle, S. (2015). Robust crack detection for unmanned aerial vehicles inspection in an
409 a-contrario decision framework. *Journal of Electronic Imaging*, 24(6), 061119.

410 Arofste, a., javidi, n., samadzadegan, f. and dadras javan, f. (2017). geometric comparison 0f key frame selection
411 techniques in 3d reconstruction based on aerial video imagery. *SMPR 2017*, Tehran.

412 Behnia, B., Buttlar, W., & Reis, H. (2018). Evaluation of low-temperature cracking performance of asphalt
413 pavements using acoustic emission: a review. *Applied Sciences*, 8(2), 306.

414 Chambon, S., Gourraud, C., Moliard, J. M., & Nicolle, P. (2010, May). Road crack extraction with adapted filtering
415 and Markov model-based segmentation: introduction and validation. In *International joint conference on*
416 *computer vision theory and applications, visapp* (p. sp).

417 Coenen, T. B., & Golroo, A. (2017). A review on automated pavement distress detection methods. *Cogent
418 Engineering*, 4(1), 1374822.

419 Cortes, C., & Vapnik, V. (1995). Support-vector networks. *Machine learning*, 20(3), 273-297.

420 Crete, F., Dolmiere, T., Ladret, P., & Nicolas, M. (2007, February). The blur effect: perception and estimation with
421 a new no-reference perceptual blur metric. In *Human vision and electronic imaging XII* (Vol. 6492, p. 64920I).
422 International Society for Optics and Photonics.

423 Cubero-Fernandez, A., Rodriguez-Lozano, F. J., Villatoro, R., Olivares, J., & Palomares, J. M. (2017). Efficient
424 pavement crack detection and classification. *EURASIP Journal on Image and Video Processing*, 2017(1), 39.

425 Ersoz, A. B., Pekcan, O., & Teke, T. (2017, September). Crack identification for rigid pavements using unmanned
426 aerial vehicles. In *IOP Conference Series: Materials Science and Engineering* (Vol. 236, No. 1, p. 012101). IOP
427 Publishing.

428 Gavilán, M., Balcones, D., Marcos, O., Llorca, D. F., Sotelo, M. A., Parra, I., ... & Amírola, A. (2011). Adaptive
429 road crack detection system by pavement classification. *Sensors*, 11(10), 9628-9657.

430 Gonzalez, R. C., & Woods, R. E. (2002). *Digital image processing* [M]. Publishing house of electronics
431 industry, 141(7).

432 Grandsaert, P. J. (2015). Integrating pavement crack detection and analysis using autonomous unmanned aerial
433 vehicle imagery (No. AFIT-ENV-MS-15-M-195). Air force institute of technology wright-patterson afb oh
434 graduate school of engineering and management.

435 Kim, H., Lee, J., Ahn, E., Cho, S., Shin, M., & Sim, S. H. (2017). Concrete crack identification using a UAV
436 incorporating hybrid image processing. *Sensors*, 17(9), 2052.

437 Koch, C., Georgieva, K., Kasireddy, V., Akinci, B., & Fieguth, P. (2015). A review on computer vision based defect
438 detection and condition assessment of concrete and asphalt civil infrastructure. *Advanced Engineering
439 Informatics*, 29(2), 196-210.

440 Mohan, A., & Poobal, S. (2018). Crack detection using image processing: A critical review and
441 analysis. *Alexandria Engineering Journal*, 57(2), 787-798.

442 Oliveira, H., & Correia, P. L. (2009, August). Automatic road crack segmentation using entropy and image
443 dynamic thresholding. In *2009 17th European Signal Processing Conference* (pp. 622-626). IEEE.

444 Quintana, M., Torres, J., & Menéndez, J. M. (2015). A simplified computer vision system for road surface
445 inspection and maintenance. *IEEE Transactions on Intelligent Transportation Systems*, 17(3), 608-619.

446 Samadzadegan, F., & Zarrinpanjeh, N. (2008). Earthquake destruction assessment of urban roads network using
447 satellite imagery and fuzzy inference systems. *The international archives of the photogrammetry, remote
448 sensing and spatial information sciences*, 37(PART B8), 409-414.

449 Sankarasrinivasan, S., Balasubramanian, E., Karthik, K., Chandrasekar, U., & Gupta, R. (2015). Health
450 monitoring of civil structures with integrated UAV and image processing system. *Procedia Computer
451 Science*, 54, 508-515.

452 Schnebele, E., Tanyu, B. F., Cervone, G., & Waters, N. (2015). Review of remote sensing methodologies for
453 pavement management and assessment. *European Transport Research Review*, 7(2), 7.

454 Yin, Z., Mao, Y., & Seto, C. (2015). Develop a uav platform for automated bridge inspection (No. 25-1121-0003-
455 295). Mid-America Transportation Center.

456 Yokoyama, S., & Matsumoto, T. (2017). Development of an automatic detector of cracks in concrete using
457 machine learning. *Procedia engineering*, 171, 1250-1255.

458 Zarrinpanjeh, N., & Dadrasjavan, F. (2017). A fuzzy automatic car detection method based on high resolution
459 satellite imagery and geodesic morphology. *International Archives of the Photogrammetry, Remote Sensing &
460 Spatial Information Sciences*, 42.